

Design of Neuro-Fuzzy Based Torque Controller for Torque Ripple Reduction of Induction Motor

A. GUNDOGDU, F. ATA and B. DANDIL

Abstract—Among all the control methods developed for Induction Motor (IM) drivers, the hysteresis controller based Direct Torque Control (DTC) method has an important place. This control method does not require other rotor and stator parameters except the stator resistance and does not require position or velocity sensors. However, there are some disadvantages of the DTC method, such as high torque, flux and current ripples. In this study, in order to reduce the high torque ripples occurring in an induction motor that is controlled by the hysteresis controller based conventional DTC method, a simple and effective Sugeno type Neuro-Fuzzy Torque Controller (NFTC) is proposed. This proposed controller is used instead of hysteresis controller. An experimental setup consisting of 1.1 kW induction motor, current and voltage measurement, DS1103 control card and two-level voltage source inverter was installed. To evaluate the performance of the proposed controller structure, various experimental studies were performed. Results obtained from the proposed NFTC based structure and conventional hysteresis controller based DTC structures are given comparatively. By the obtained experimental results, it was confirmed that the proposed NFTC-based controller structure considerably reduced flux and torque ripples in the motor.

Index Terms—Direct Torque Control, AC Drives, Neural Fuzzy Networks, Torque Ripple Reduction.

I. INTRODUCTION

ASYNCHRONOUS MOTORS have been largely used for many years because of their simple structure, high-strength, reliability, robustness, low cost, and high efficiency. In industrial applications, different methods have been used to

AHMET GUNDOGDU, is with Department of Electrical Engineering University of Batman, Turkey, (e-mail: ahmet.gundogdu@batman.edu.tr).

 <https://orcid.org/0000-0002-8333-3083>

FIKRET ATA, is with Department of Electrical Engineering University of Bingol, Bingol, Turkey, (e-mail: fata@bingol.edu.tr).

 <https://orcid.org/0000-0000-0000-0000>

BESIR DANDIL, is with Department of Mechatronics Engineering University of Firat, Elazig, Turkey, (e-mail: bdandil@firat.edu.tr).

 <https://orcid.org/0000-0002-3625-5027>

Manuscript received April 30, 2020; accepted May 28, 2020.
DOI: 10.17694/bajece.730311

control induction motors. These methods are generally implemented in two ways, vector and scalar control methods. In the scalar method, only the frequency and amplitude of current, voltage and flux space vectors are controlled. On the other hand, in the vector control method, in addition to the amplitude and frequency, the positions of these current, voltage and flux vectors are also checked [1,18]. To be able to achieve a high-performance control of the variable-speed induction motor drivers, the vector control method can be used. Vector control method ensures decoupled control of torque and flux independently of each other as in a free-excitation direct current machine.

There are two most widely used vector control methods, Direct Torque Control (DTC) and Field Oriented Control (FOC). As first, the Field Oriented Control was proposed by Blaschke [2] in 1971. Development of the conventional Direct Torque Control (DTC) was carried out by Takahashi [3] in 1986. Direct Torque Control method (DTC) has some characters such as simple control structure, high-speed torque and flux response, and robustness against parameter uncertainties [4,5]. Compared to the Field Oriented Control method, it is seen that the DTC method is less sensitive to parameter changes.

However, the conventional DTC method has some disadvantages, such as high torque, flux and current fluctuations, high acoustical noise level at low speed, variable switching frequency, difficulty in the control of flux and torque at very low speeds, and nonzero steady state torque error [6]. To be able to solve the above mentioned disadvantages of the conventional DTC, many research have been carried out by researchers on adaptive hysteresis band [5], improved switching table [7,8], space vector modulation approach and constant switching frequency [9,10,25], reduction of torque ripple [7-10,22,23], Intelligent control techniques [11,12], complex flux estimation methods [13], controller design [9,14,26,27], multilevel inverters [15], predictive control [16], genetic algorithm [19], parameter estimation with particle swarm optimization [20]. There are two fundamental problems that many researchers have been focusing on; these are high torque ripple and variable switching frequency. Different application schemes based on intelligent control techniques (e.g., fuzzy logic, genetic algorithm, neural networks, and neural-fuzzy) have been proposed to overcome these problems [21, 24].

In this study, in order to decrease the high torque ripple and obtain a switching frequency that was constant, a new Neuro-

Fuzzy Torque Controller (NFTC), which was in Sugeno type, was proposed. Torque error and the change of torque error were selected as input variables of NFTC. The output variable of this controller is the torque slope (T_{SLP}). In the 2nd part of this paper, a dynamic model of an IM is presented. In the 3rd part, torque and flux equations related to the conventional DTC is given. In part 4, the internal structure of the proposed controller is described. Finally, in the 5th part, the block diagram for the experimental design and experimental results are given.

II. THE DYNAMIC MODEL FOR AN INDUCTION MOTOR

It is possible to give the dynamic model of an IM on the stationary reference frame as below.

Stator voltage equations:

$$V_{s\alpha} = \frac{d}{dt} \varphi_{s\alpha} + R_s I_{s\alpha} \quad (1)$$

$$V_{s\beta} = \frac{d}{dt} \varphi_{s\beta} + R_s I_{s\beta} \quad (2)$$

$$\bar{V}_s = \frac{d}{dt} \bar{\varphi}_s + R_s \bar{I}_s \quad (3)$$

Stator flux equations:

$$\varphi_{s\alpha} = L_s I_{s\alpha} + L_m I_{r\alpha} \quad (4)$$

$$\varphi_{s\beta} = L_s I_{s\beta} + L_m I_{r\beta} \quad (5)$$

$$\bar{\varphi}_s = L_s \bar{I}_s + L_m \bar{I}_r \quad (6)$$

Rotor flux equations:

$$\varphi_{r\alpha} = L_r I_{r\alpha} + L_m I_{s\alpha} \quad (7)$$

$$\varphi_{r\beta} = L_r I_{r\beta} + L_m I_{s\beta} \quad (8)$$

$$\bar{\varphi}_r = L_r \bar{I}_r + L_m \bar{I}_s \quad (9)$$

In equations (1)-(9), the notations of "s" and "r" refer to the stator and rotor variables, respectively. In addition, while the stator voltages are referred by $V_{s\alpha}$ and $V_{s\beta}$, $I_{s\alpha}$ and $I_{s\beta}$ refer to stator currents, $I_{r\alpha}$ and $I_{r\beta}$ refer to rotor currents, $\varphi_{s\alpha}$ and $\varphi_{s\beta}$ refer to stator fluxes, $\varphi_{r\alpha}$ and $\varphi_{r\beta}$ refer to rotor fluxes, I_s and I_r refer to stator and rotor current vectors, R_s refers to stator winding resistance, and L_s , L_r , L_m refer to the stator and rotor inductance and common inductances of them. The motor's electromagnetic torque (T_e) can be derived as in Equations (10)-(11) by using stator and rotor flux equations given above.

$$T_e = \frac{3P}{2} \frac{L_m}{\sigma L_s L_r} \bar{\varphi}_s * \bar{\varphi}_r \quad (10)$$

$$T_e = \frac{3P}{2} \frac{L_m}{\sigma L_s L_r} |\bar{\varphi}_s| \cdot |\bar{\varphi}_r| \cdot \sin(\gamma_s - \gamma_r) \quad (11)$$

$$\gamma_s - \gamma_r = \delta \quad (12)$$

In this equation, $\sigma = 1 - L_m^2/L_s L_r$ is the leakage factor, P is the number of double poles, γ_s, γ_r are rotor and stator flux vectors' angles, and δ is the torque angle. In equation (11), it is obviously seen that the electromagnetic torque generated by the motor is a function of the rotor and stator flux vectors. The relationship between rotor and stator flux vectors is demonstrated in Figure 1. A sudden change is followed by the rotor flux in the rotor flux $\bar{\varphi}_s$ with a certain delay. The generated electromagnetic torque is proportional to $|\bar{\varphi}_s|, |\bar{\varphi}_r|$ and torque angle δ .

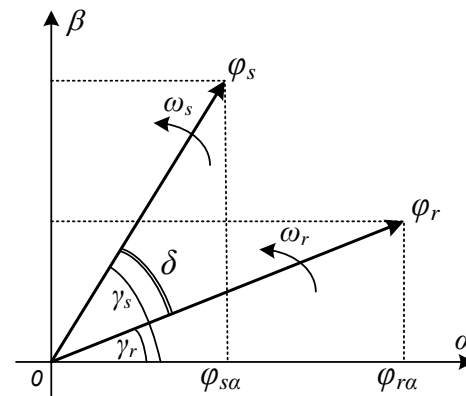


Figure 1. Rotor and stator flux vectors in $\alpha\beta$ reference frame.

According to Figure 1, it is possible to realize the torque control of the IM via controlling the torque angle δ . In a balanced continuous sinusoidal situation, depending on operating conditions, the rotation of the rotor and stator flux vectors at a constant angular speed is observed. In this case, the torque angle δ is constant and this depends on the operating conditions. Thus, the generated electromagnetic torque becomes constant. If the flux vector $|\bar{\varphi}_s|$ accelerates, the torque angle δ and the generated electromagnetic torque increase. If the flux vector $|\bar{\varphi}_s|$ slows down, the torque angle δ and the generated torque reduce.

III. TORQUE AND FLUX EQUATIONS OF CONVENTIONAL DIRECT TORQUE CONTROL METHOD

The conventional DTC method achieves decoupled control of the electromagnetic torque and the stator flux independently from each other. The fundamental principle of this method is regulating the amplitude of the stator flux and the electromagnetic torque by selecting directly the appropriate voltage vectors and their control signals. To estimate the components of the stator flux, the stator voltage model is used. Stator voltage model is generally a simple form of stator flux

estimation techniques. Following equations are used in order to calculate the components and amplitudes of the stator flux;

$$\varphi_{s\alpha} = \int (V_{s\alpha} - R_s I_{s\alpha}) dt \quad (13)$$

$$\varphi_{s\beta} = \int (V_{s\beta} - R_s I_{s\beta}) dt \quad (14)$$

$$\varphi_s = \sqrt{\varphi_{s\alpha}^2 + \varphi_{s\beta}^2} \quad (15)$$

In a practical application, stator voltage components ($V_{s\alpha}$, $V_{s\beta}$) and stator current components ($I_{s\alpha}$, $I_{s\beta}$) are obtained by applying the $\alpha\beta$ conversion to the real 3~ voltage and currents measured from the motor terminals.

In order for estimation, only stator voltage, resistance and current are required and this estimation depends on open-loop integration of the stator back-emf. Through this way,

estimation of the flux is ensured accurately at high speeds. On the other hand, noise in voltage and current measurement, stator resistance voltage drop and integration drift become significant because it causes an inaccurate estimation at low speed.

As it is presented in the equation (16), the electromagnetic torque, which the motor generates, is calculated with the help of the stator flux and currents.

$$T = \frac{3}{2} P (\varphi_{s\alpha} I_{s\beta} - \varphi_{s\beta} I_{s\alpha}) \quad (16)$$

The fundamental control diagram for the conventional DTC method proposed by Takahashi for induction motor drivers is given in Figure 2. This control structure includes torque and torque with flux hysteresis tapes, flux and angle estimation blocks, and a switching table for selection of voltage vectors.

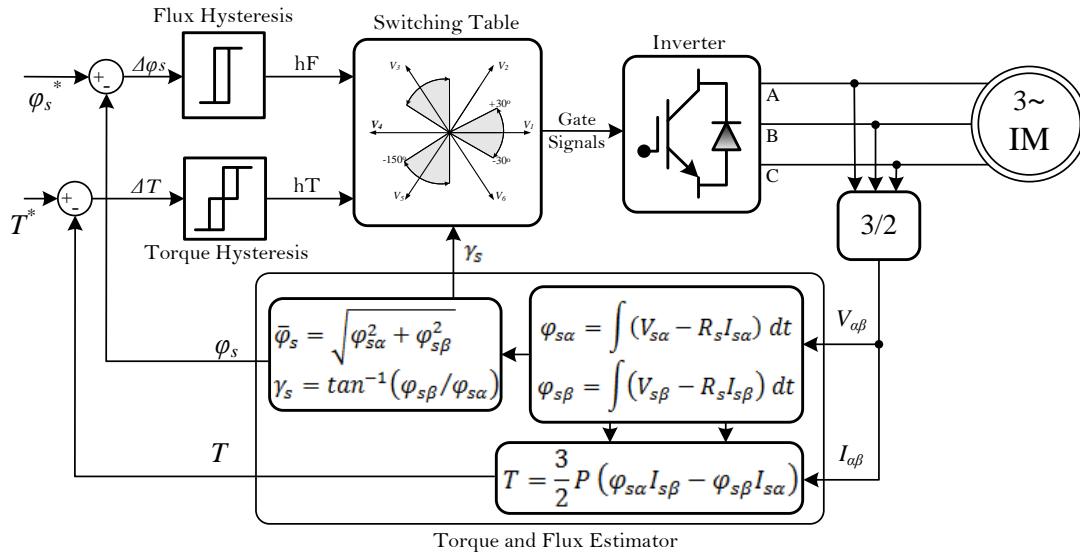


Figure 2. Basic configuration of the conventional DTC

As shown in Figure 2, there are two different cycles in which flux and torque are obtained. In the conventional DTC method, when the closed-loop process of motor driver system is performed, a PI speed controller is usually utilized for the generation of the reference torque. Torque error ΔT and flux error $\Delta\varphi_s$ are obtained by comparing the torque and flux reference values with their actual values obtained by the measurement.

$$\Delta T = T^* - T \quad (17)$$

$$\Delta\varphi_s = \varphi_s^* - \varphi_s \quad (18)$$

$$\gamma_s = \tan^{-1}(\varphi_{s\beta} / \varphi_{s\alpha}) \quad (19)$$

In the equations (17) - (19) above, T^* is reference torque, φ_s^* is reference current and γ_s is the stator flux vector angle. The inverter switching signals are obtained by helping of ΔT , $\Delta\varphi_s$ and γ_s . The torque and flux errors obtained at the output of the comparison blocks are applied as input to hysteresis controllers. While the flux hysteresis controller is a two-level comparator, the torque hysteresis controller is a three-level comparator.

While the flux hysteresis controller generates $hF=1$, $hF=0$ at the output according to the flux error information at the input, the torque hysteresis controller generates $hT=-1$, $hT=0$, $hT=1$ at the output according to the torque error information at the input. These numerical values are then applied as input to the switching table for determining the region where the stator flux vector is located. The switching table is presented in Table 1.

TABLE I
TAKAHASHI SWITCHING TABLE

hF	hT	N=1	N=2	N=3	N=4	N=5	N=6
1↑	1↑	V2	V3	V4	V5	V6	V1
	0	V7	V0	V7	V0	V7	V0
	-1↓	V6	V1	V2	V3	V4	V5
0↓	1↑	V3	V4	V5	V6	V1	V2
	0	V0	V7	V0	V7	V0	V7
	-1↓	V5	V6	V1	V2	V3	V4

The orbit of the stator flux vector is divided into six different sectors. The voltage source inverter generates a total of eight voltage vectors; six active voltage vectors (V1-V6) and two zero voltage vectors (V0-V7). Representations of these voltage vectors and sectors on αβ frame are given in Figure 3.

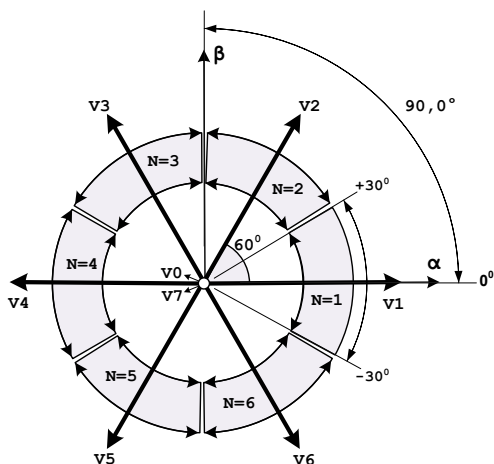


Figure 3. Inverter voltage vectors and sectors.

N=1-6 number sectors that includes the stator flux vector is determined by equation (20), and the angular position of this flux vector is determined by equation (19).

$$-\frac{\pi}{6} + (N - 1) \frac{\pi}{3} \leq \gamma_s(N) < \frac{\pi}{6} - (1 - N) \frac{\pi}{3} \quad (20)$$

Depending on the hysteresis flux controllers and output of the hysteresis torque, the most suitable voltage vectors are selected from Table 1. According to Table 1, the flux decreases for hF=0 and the flux increases for hF=1. Similarly, the torque increases for hT=1, the torque decreases for hT=-1 and the torque does not change for hT=0.

IV. PROPOSED NEURO-FUZZY TORQUE CONTROLLER

In order for designing of the Neuro-Fuzzy Torque Controller, Artificial Neural Networks and Fuzzy Logic are able to be used together. To be able to obtain the first artificial neural network structure, online/offline learning processes can be used with the help of human expert knowledge. For combining artificial neural networks and fuzzy logic, one of the recommended methods is the adaptive neuro-fuzzy inference system (ANFIS) [11,12]. Instead of the torque hysteresis controller used in the conventional DTC method, a neuro-fuzzy torque controller whose block diagram is given in

Figure 4 is used in this study. The proposed controller performs the same task as the conventional three-level torque hysteresis controller. For this reason, the same switching table is used for selecting the appropriate voltage vectors.

The proposed structure of the neuro-fuzzy torque controller is presented in Figure 4. This controller structure consists of two triangular carrier waves [9], two comparator blocks and a neuro-fuzzy controller. Triangular carrier waves (carr_upp and carr_low) have 180° phase difference.

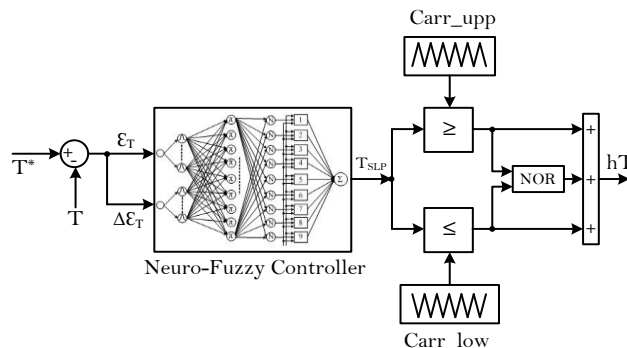


Figure 4. Proposed neuro-fuzzy torque controller.

The internal structure of the proposed neuro-fuzzy torque controller is demonstrated in Figure 5.

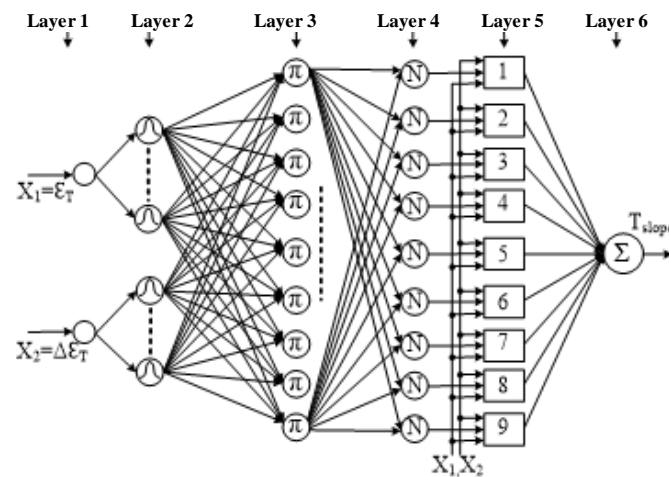


Figure 5. Two-input neuro-fuzzy controller structure.

The input variables of the controller are the torque error and the variation of this error. In addition, the torque slope T_SLP is the output variable of the controller. This controller is a first order sugeno type controller. It consists of functional blocks constructed by using six network layers: The layers of the controller perform fuzzification, inference and defuzzification of the fuzzy systems.

LAYER 1. In this layer, the input of the controller is selected as, X₁=ε_T(t), X₂=Δε_T(t)

LAYER 2. This layer contains the membership functions. For input variables, calculation of membership function degree is done by this layer.

LAYER 3. This layer applies the fuzzy as well as the operation. Here, the output specifies the firing strength of the rules.

LAYER 4. Here, respecting to the others, each input is being normalized.

LAYER 5. In this layer, the calculation of the consequent values is performed. Here, the output is the result of the normalized certainty of a rule and the function related to this.

LAYER 6. This is the output layer. Here, an output is generated as a collection of all incoming signals.

The torque slope T_{SLP} , which is the output of the neuro-fuzzy controller, is compared to the triangular carrier wave as shown in Figure 6.

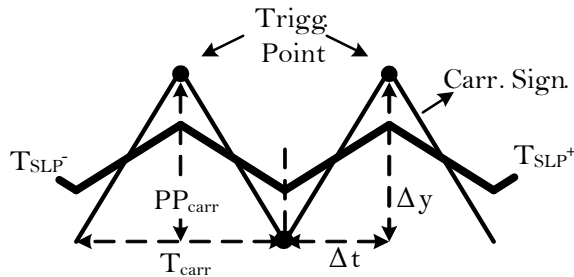


Figure 6. Triangle carrier signal and torque.

Here, PP_{car} is the top-to-top value of the triangular carrier wave and T_{car} is its period. The slope of the triangular carrier wave is calculated as in equation (21).

$$\begin{aligned} |absolute\ slope_{carr}| &= \frac{\Delta y}{\Delta t} = \frac{PP_{carr}}{T_{carr}/2} \\ &= 2f_{carr} PP_{carr} \end{aligned} \quad (21)$$

In reference [17], it is emphasized that the torque slope, the motor speed, rotor and stator fluxes, stator voltage are functions of load. The expressions for the increasing in torque (T_{SLP}^+) and the decreasing in torque (T_{SLP}^-) are given in the equations (22) and (23).

$$\begin{aligned} T_{SLP}^+ &= \frac{dT^+}{dt} = -A_t T + B_t V_s^{\phi_s} \\ &\quad + K_t \left(\frac{w_e}{d} - w_r \right) \end{aligned} \quad (22)$$

$$T_{SLP}^- = \frac{dT^-}{dt} = -A_t T - K_t w_r \quad (23)$$

where,

$$A_t = \frac{1}{\sigma \tau_{sr}} \quad (24)$$

$$B_t = \frac{3P}{2} \frac{L_m}{\sigma L_s L_r} \phi_r \quad (25)$$

$$K_t = \frac{3P}{2} \frac{L_m}{\sigma L_s L_r} (\phi_s \phi_r) \quad (26)$$

The absolute slope of the T_{SLP} should not exceed the absolute slope of the triangular carrier signal.

$$T_{SLP} \leq \frac{\Delta y}{\Delta t} = \frac{PP_{carr}}{T_{carr}/2} = 2f_{carr} PP_{carr} \quad (27)$$

The slope of the T_{SLP} in the neuro-fuzzy controller is determined by the scaling factor K_{SF} . On the other side, the scaling factor K_{SF} is obtained by using equations (22) and (23) as below.

For the positive slope, from Eq.(22);

$$K_{SF}^+ \leq \frac{2f_{carr} PP_{carr}}{T_{SLP}^+} \quad (28)$$

For the negative slope, from Eq.(23);

$$K_{SF}^- \leq \frac{2f_{carr} PP_{carr}}{|T_{SLP}^-|} \quad (29)$$

are obtained. The output of the proposed neuro-fuzzy torque controller (hT) is given by equation (30) and it is the same as the outputs of the three-level torque hysteresis controller,

$$hT = \begin{cases} 1 & T_{SLP} \geq carr_upp \\ 0 & carr_low < T_{SLP} < carr_upp \\ -1 & T_{SLP} \leq carr_low \end{cases} \quad (30)$$

In addition, a flux controller is designed using a proportional gain instead of neuro-fuzzy controller or similar torque controller.

V. EXPERIMENTAL SETUP AND RESULTS

A block diagram of the experimental setup developed to implement both the conventional hysteresis controller based DTC method and the proposed neuro-fuzzy torque controller based DTC method is given in Figure 7.

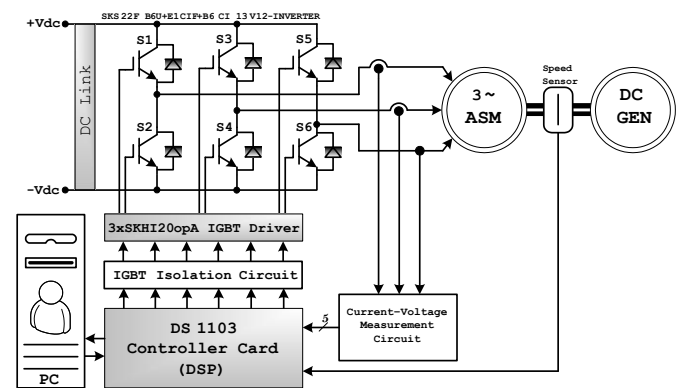


Figure 7. Block diagram of experimental setup.

The experimental setup consists of dSPACE DS1103 control card, 5000 pulse incremental encoder, Semikron SKS22F B6U model, three-phased VSI-IGBT inverter and 2-pole, 1.1 kW, 380 V, 50 Hz standard induction motor whose parameters are given in Appendix A. Figure 9 shows a photo related to the experimental setup. The DS1103 control card has PowerPC PPC750GX/1 GHz master processor and TMS320F240/20 MHz auxiliary processor.

By the help of the measured stator currents and voltages, estimation of the torque and flux, generation of the triangular carrier waves, determination of the sector where the flux vector is located, realization of the numerical calculation of the neuro-fuzzy controller and all other calculations are performed by using this control card. The control algorithm for the proposed controller structure was carried out by using the Matlab/Simulink block diagram presented in Figure 8.

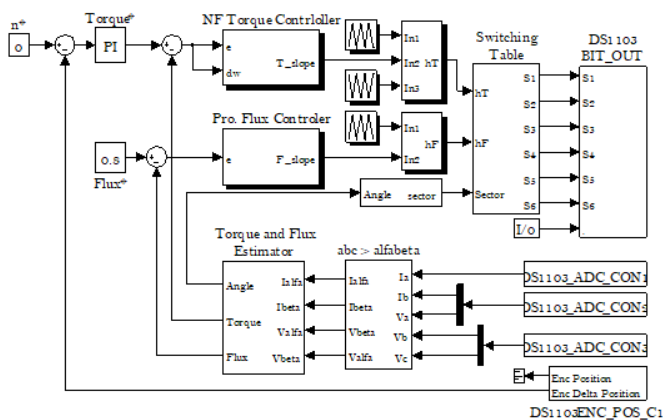


Figure 8. Matlab/Simulink block diagram of the proposed DTC with NFTC.

User interface software called Control Desk Developer (CDD) was used to display real-time measurements such as motor speed, stator voltages and currents, and to change the speed reference and controller parameters online.



Figure 9. Photograph of the experimental setup.

In the experimental studies, it was determined that the DC bus voltage of the inverter was 520 volts, the dead time was $3 \mu\text{s}$, the sampling period was $T_s=50\mu\text{s}$ and the period of the triangular carrier signal for the torque cycle is $T_{\text{carr}}=100 \mu\text{s}$. By PI speed controller, the starting torque of the motor was limited as $\pm 6 \text{ Nm}$.

Torque hysteresis controller was set to 10% of nominal torque so that its bandwidth was 0.372 Nm. The real value of the stator flux was calculated using the stator voltage model. Its reference value was 0.8 Wb.

The flux hysteresis controller was set to 1% of the nominal flux so that its bandwidth was 0.008 Wb. The motor shaft speed was measured with a high-resolution encoder of 5000 pulses. To load the motor, a DC generator was installed on the motor shaft. Measurement of the two-phase currents were performed by two Hall-effect current sensors and the third phase current was obtained by calculation in the algorithm. The measurement of the motor peak voltages are also done by Hall-effect voltage sensors and transferred into the control structure.

Various experimental studies were carried out in order to show the performance of the proposed neuro-fuzzy torque controller, and for the both control methods, the obtained results are given below.

A. Transient Performance

The transient regime performance of the both control algorithms under the same operating conditions was analyzed by comparing torque, speed, flux and current responses. First, the graphs obtained for the unloaded state of the motor are given in Figures (10)-(11).

The speed and torque responses of the two control algorithms are shown in Figure 10. With regards to the settling time of speed and torque, transient performances are similar. Figure 11 presents speed, torque, current and flux responses obtained using proposed NFTC algorithm for the speed reversal from -2700 rpm to +2700 rpm and from +2700 rpm to -2700 rpm. The torque and phase current increased during reversal operation mode.

During this time, the amplitude of the stator flux is being fixed at 0.8 Wb. This result verifies that decoupling process between the flux and torque can deal with the four-quadrant operation mode.

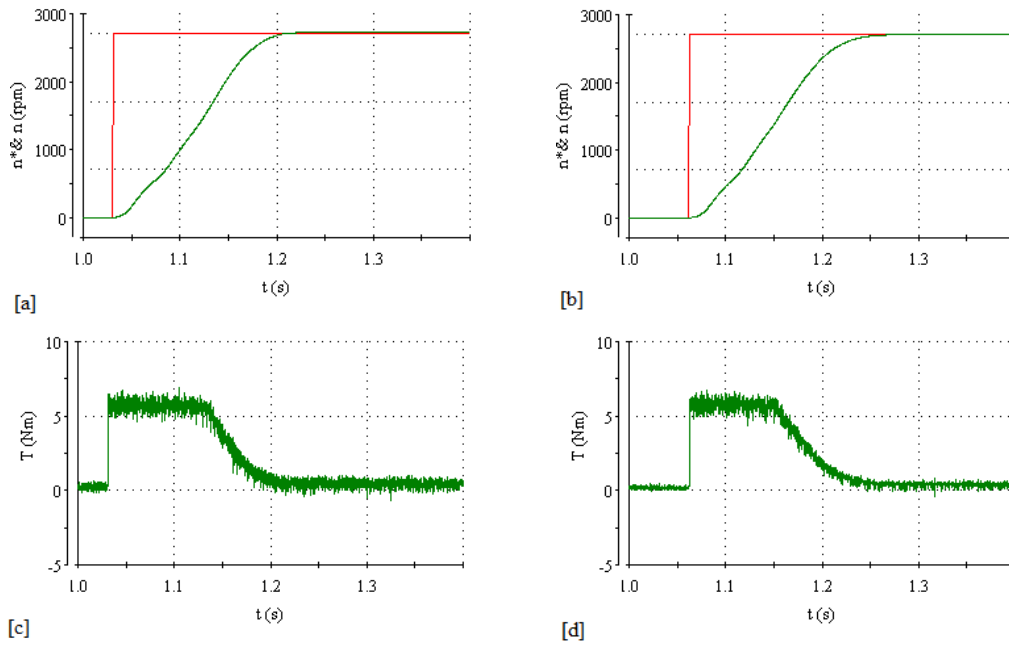


Figure 10. Experimental responses, no-load, from 0 to 2700 rpm. (a) Speed response for conventional DTC. (b) Speed response for Proposed DTC. (c) Torque response for conventional DTC. (d) Torque response for Proposed DTC.

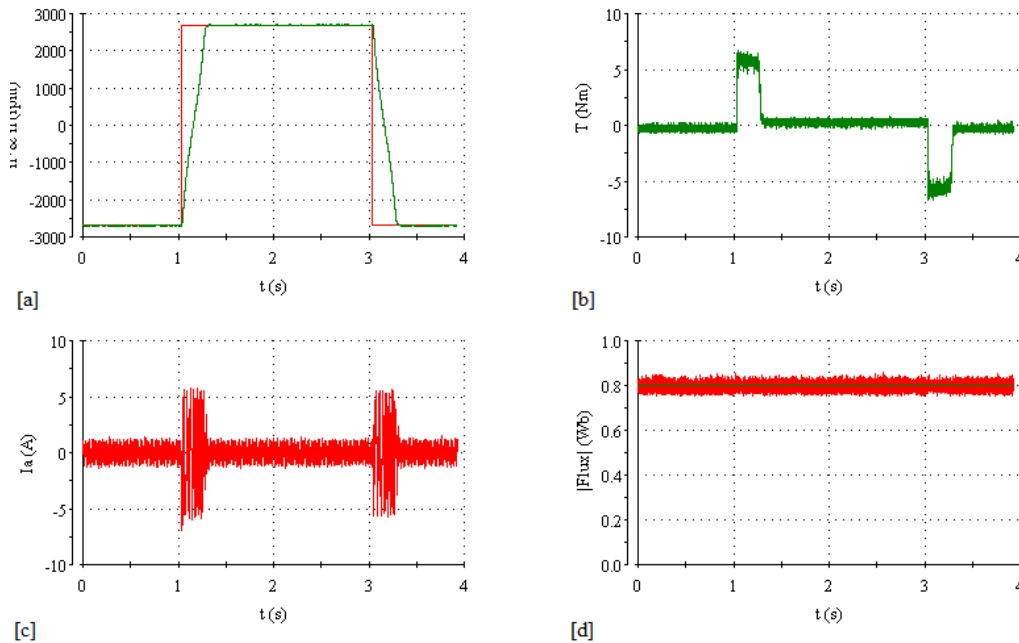


Figure 11. Experimental responses for Proposed DTC, no-load, from -2700 to +2700 rpm. (a) speed, (b) torque, (c) current, (d) flux.

B. Steady-State Performance

Evaluating the torque, speed, flux and current ripples in different conditions, the steady state performance of the two control algorithms was compared. Graphics of the steady states are presented in Figures 12-18, for no-load and with-load operation at +2700 rpm.

Figure 12 (a) and (b) demonstrates the experimental torque responses. The related rms torque ripples of the conventional DTC algorithm and proposed NFTC algorithm are 1.8 and 0.9 Nm., respectively. It is understood that a reduction in the rms

torque ripple is small noticeably. Compared with the conventional DTC, this rms torque ripple level is significantly decreased.

Moreover, except torque ripple, speed and flux responses are presented in Figures 13 and 14, respectively. Figure 13 (a) and (b) show the experimental rms speed ripples of 10 and 5 rpm for the conventional DTC and proposed NFTC algorithm, respectively. Figure 14 (a) and (b) show the experimental rms flux ripples of 0.1100 and 0.0974 Wb for the conventional

DTC and proposed NFTC algorithm, respectively. It is seen that rms speed and flux ripples are reduced.

As shown in Figures 15 and 16, the stator phase current and $\alpha\beta$ currents are nearly sinusoidal. The amplitude of current ripples in NFTC is lower than that of conventional DTC. On the other hand, in the NFTC algorithm, the oscillations are more regular and uniform.

Figures 17 and 18 show the stator $\alpha\beta$ fluxes waveform and its circular trajectory. Compared the speed, torque, current, and flux responses of the experimental results given in Figures 12-18, it can be seen that the proposed NFTC algorithm has decreased not only the torque ripple but also the speed, flux, and current ripples.

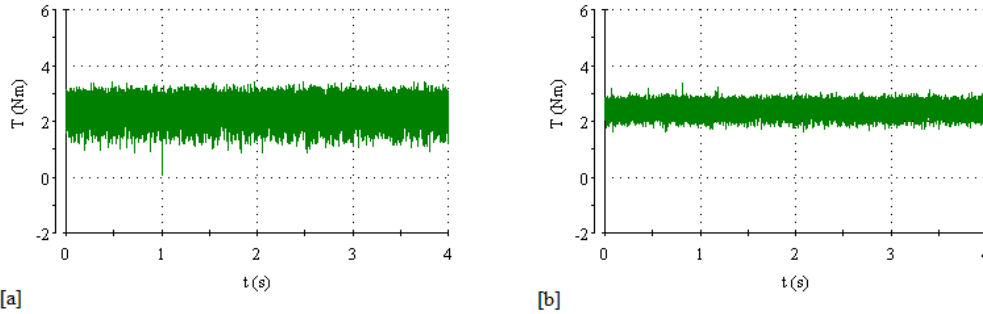


Figure 12. Experimental torque responses, with-load, at +2700 rpm. (a) Conventional DTC. (b) Proposed DTC

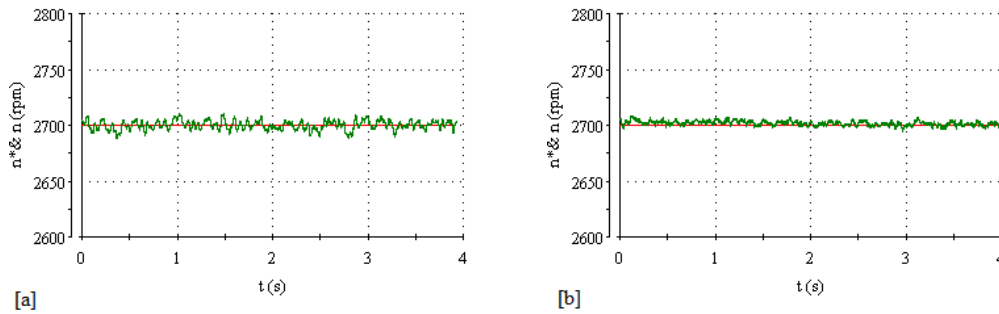


Figure 13. Experimental speed responses, no-load, at +2700 rpm. (a) Conventional DTC. (b) Proposed DTC.

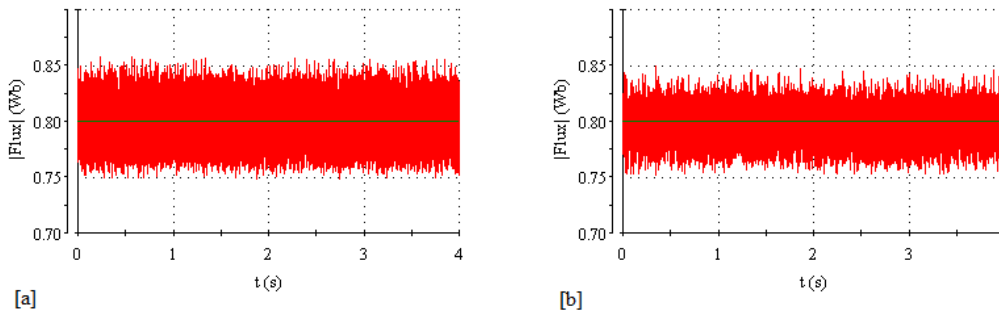


Figure 14. Experimental |Flux| responses, with-load, at +2700 rpm. (a) Conventional DTC. (b) Proposed DTC.

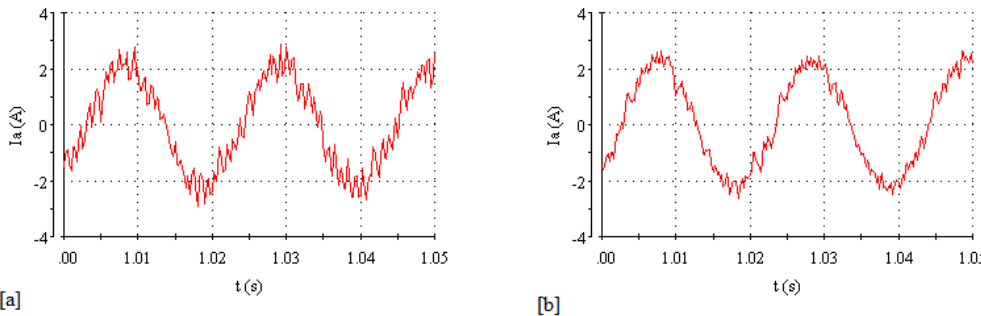


Figure 15. Experimental phase current responses, with-load, at +2700 rpm. (a) Conventional DTC. (b) Proposed DTC.

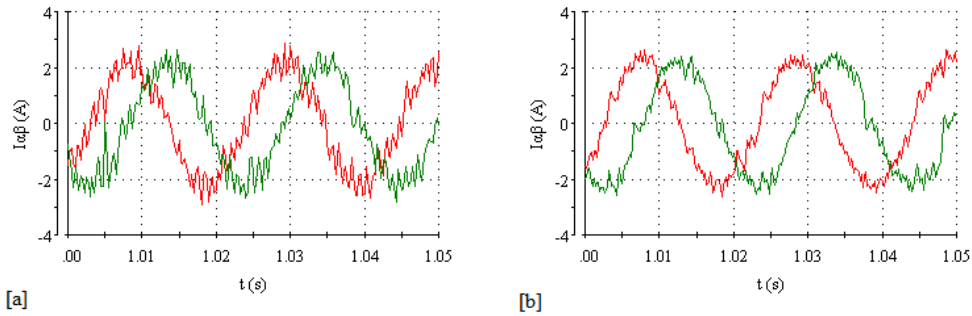


Figure 16. Experimental $\alpha\beta$ current responses, with-load, at +2700 rpm. (a) Conventional DTC. (b) Proposed DTC.

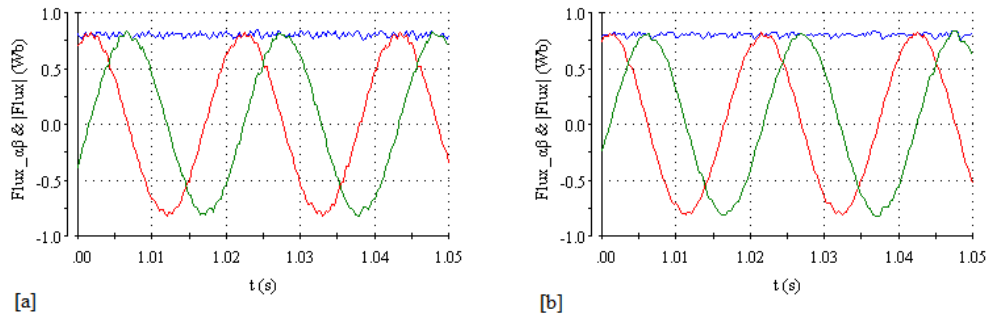


Figure 17. Experimental $\alpha\beta$ flux responses, with-load, at +2700 rpm. (a) Conventional DTC. (b) Proposed DTC.

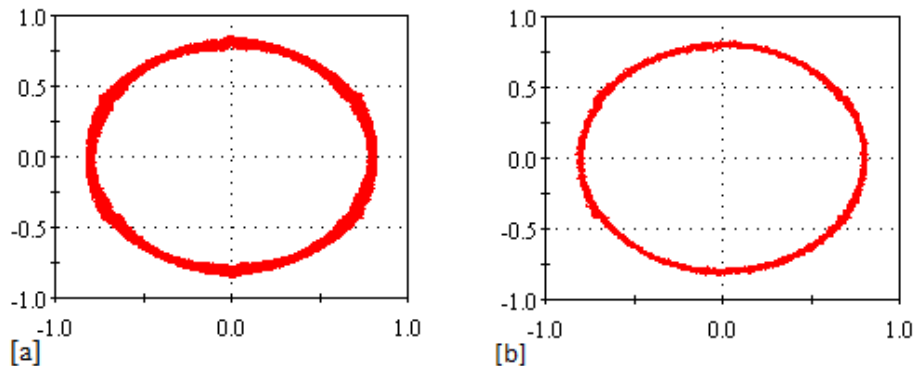


Figure 18. Experimental stator flux trajectory responses, with-load, at +2700 rpm. (a) Conventional DTC. (b) Proposed DTC

VI. CONCLUSION

Although the DTC is preferred for highly dynamic applications, it shows high torque and current ripple. In this study, a new neuro-fuzzy torque controller is proposed in order to enhance the performance of the conventional DTC and to reduce torque ripples. The efficiency of the proposed controller is demonstrated experimentally under the step speed and load changes. Looking at the experimental results, it is seen that the proposed neuro-fuzzy torque controller has a few advantages, such as torque and flux ripple reduction, low harmonic contents for currents, good performance at low-speed range, sinusoidal stator currents, and constant switching frequency. However, the performance of the controller is highly determined by the quality of the calculation of the scaling factor K_{SF} . It should be noted that the values of K_{SF} , are not optimized for all speed ranges. The scaling factor must be optimized using by advanced control techniques.

As a result of this study, transient performances of two control algorithms are similar, but the steady-state performance of the proposed NFTC control algorithm is better than the conventional DTC. While it maintains the simple structure of the DTC at the same time, the proposed neuro-fuzzy torque controller produces lower torque, speed, flux, and current ripples when compared with the conventional DTC. It is seen that the torque, speed, flux, and current ripples are significantly decreased.

ACKNOWLEDGEMENT

This study is a part of Ahmet GÜNDOĞDU's doctorate thesis, and it is supported by Firat University Scientific Research Projects Unit (FUBAP) with 1724 numbered project, titled "Torque Ripple Reduction by Neural-Fuzzy Networks of Asynchronous Motor."

APPENDIX

Motor Parameters;

3 Phase; P=1.1 kW; V=220 V; f=50 Hz; 2P=2; Rs=8.231 Ω; Rr=4.46 Ω; Lm=0.5787 mH; J=0.0019 kg.m²; B=0.000263 Nms

REFERENCES

- [1] Buja G, Kazmierkowski MP. "Direct Torque Control of PWM Inverter Fed AC Motors-A Survey". *IEEE Transactions on Industrial Electronics*, 51 (4), 744-757, 2004.
- [2] Blaschke F. "A New Method for the Structural Decoupling of AC Induction Machines". *In Conf. Rec. IFAC*, 1-15, 1971.
- [3] Takahashi I, Noguchi T. "A New Quick-Response and High Efficiency Control Strategy of an Induction Machine". *IEEE Transactions on Industrial Applications*, 22, 820-827, 1986.
- [4] Belkacem S, Naceri F, Abdessemed R. "Reduction of Torque Ripple in DTC for Induction Motor Using Input-Output Feedback Linearization". *Turkish Journal of Electrical Engineering and Computer Sciences*, 20(3), 273-285, 2012.
- [5] Casadei D, Grandi G, Serra G, Tani A. "Effects of Flux and Torque Hysteresis Band Amplitude in Direct Torque Control of Induction Machines". *In Conf. Rec. IECON'94*, 299-304, 1994.
- [6] Casadei D, Profumo F, Serra G, Tani A. "FOC and DTC: Two Viable Schemes for Induction Motors Torque Control". *IEEE Transactions on Industrial Electronics*, 17 (5), 779-787, 2002.
- [7] Casadei D, Serra G, Tani A. "Improvement of Direct Torque Control Performance by Using a Discrete SVM Technique". *In Conf. Rec. PESC'98*, 997-1003, 1998.
- [8] Galvan E, Carrasco JM, Ortega R, Escobar G, Stankovic AM. "A Family of Switching Control Strategies for the Reduction of Torque Ripple on the Direct Torque and Flux Control for Induction Motors". *The 27th Annual Conference of the IEEE Industrial Electronics Society*, 1274-1279, 2001.
- [9] Idris NRN, Yatim AHM. "A Reduced Torque Ripple Controller for Direct Torque Control of Induction Machines". *Electric Power Components and Systems*, 507-524, 2002.
- [10] Tripathi A, Khambadkone AM, Panda SK. "Torque Ripple Analysis and Dynamic Performance of a Space Vector Modulation Based Control Method for AC-Drives". *IEEE Transactions on Power Electronics*, 20(2), 485-492, 2005.
- [11] Grabowski PZ, Blaabjerg F. "Direct Torque Neuro-Fuzzy Control of Induction Motor Drive". *DSP Implementation In Conf. Rec. IECON'98*, 657-661, 1998.
- [12] Vasudevan M, Arumugam R. "High-Performance Adaptive Intelligent Direct Torque Control Schemes for Induction Motor Drives". *KMITL Sci. Tech. J*, 5(3), 559-576, 2005.
- [13] Xia Y, Oghanna W. "Fuzzy Direct Torque Control of Induction Motor with Stator Flux Estimation Compensation". *In Proc. IEEE IECON'97*, 2, 505-510, 1997.
- [14] Lai YS, Lin JC. "New Hybrid Fuzzy Controller for Direct Torque Control Induction Motor Drives". *IEEE Transactions on Power Electronics*, 18(5), 1211-1219, 2003.
- [15] Lee KB, Song JH. "Torque Ripple Reduction in DTC of Induction Motor Driven by Three-Level Inverter With Low Switching Frequency". *IEEE Transactions on Power Electronics*, 17(2), 255-264, 2002.
- [16] Miranda H, Cortes P, Yuz P, Rodriguez J. "Predictive Torque Control of Induction Machines Based on State-Space Models". *IEEE Transactions on Industrial Electronics*, 56(6), 1916-1924, 2009.
- [17] Kang JK, Sul SK. "Torque Ripple Minimization Strategy for Direct Torque Control of Induction Motor". *In Conf. Rec. IEEE-IAS*, 438-443, 1998.
- [18] Qutubuddin MD, Yadaiah N. "Modeling and Implementation of Brain Emotional Controller for Permanent Magnet Synchronous Motor Drive". *Engineering Applications of Artificial Intelligence*, 60, 193-203, 2017.
- [19] Sangdani MH, Tavakolpour-Saleh AR, Lotfavar A. "Genetic Algorithm-Based Optimal Computed Torque Control of a Vision-Based Tracker Robot: Simulation and Experimental". *Engineering Applications of Artificial Intelligence*, 67, 24-38, 2018.
- [20] Sakthivel VP, Bhuvaneswari R, Subramanian S. "Multi-Objective Parameter Estimation of Induction Motor Using Particle Swarm

Optimization". *Engineering Applications of Artificial Intelligence*, 23, 302-312, 2010.

- [21] Kumar RH, Iqbal A, Lenin NC. "Review of Recent Advancements of Direct Torque Control in Induction Motor Drives-A Decade of Progress". *IET Power Electronics*, 11(1), 1-15, 2018.
- [22] Gowri KS, Reddy TB, Babu CS. "Direct Torque Control of Induction Motor Based on Advanced Discontinuous PWM Algorithm for Reduced Current Ripple". *Electrical Engineering*, 92, 245-255, 2010.
- [23] Labiod C, Srairi K, Mahdad B, Benbouzid MEH. "A Novel Control Technique for Torque Ripple Minimization in Switched Reluctance Motor Through Destructive Interference". *Electrical Engineering*, 100(2), 481-490, 2018.
- [24] Kesler S, Akpınar AS, Saygın A. "The Fuzzy Logic Based Power Injection Into Rotor Circuit For Instantaneous High Torque And Speed Control In Induction Machines". *Pamukkale University Journal of Engineering Sciences*, 15(1), 13-23, 2009.
- [25] Zaky MS. "High Performance DTC of Induction Motor Drives Over a Wide Speed Range". *Electrical Engineering*, 97(2), 139-154, 2015.
- [26] Deniz E, Coteli R, Dandil B, Tuncer S, Ata F, Gencoglu MT. "Neuro-Fuzzy Current Controller for Three-Level Cascade Inverter Based D-STATCOM". *45th International Universities Power Engineering Conf. UPEC'2010*, 1-5, 2010.
- [27] Coteli R, Deniz E, Dandil B, Tuncer S, Ata F. "Phase Angle Control of Three Level Inverter Based D-STATCOM Using Neuro-Fuzzy Controller". *Advances in Electrical and Computer Engineering*, 12(1), 77-84, 2012.

BIOGRAPHIES



AHMET GUNDOGDU, Elazığ in 1974. He received the B.S. and M.S. degrees in electrical teaching from the University of Firat, Elazığ, in 2004 and the Ph.D. degree in electrical engineering from Firat University, Elazığ, in 2012. From 2000 to 2012, he was a Research Assistant with the electrical teaching department. Since 2013, he has been an Assistant Professor with the Electrical Engineering Department, Batman University. His research interests include magnetic levitation, electrical machines, motor control.



FIKRET ATA, Department of Electrical Engineering, Bingol University.



BEŞİR DANDİL, Department of Mechatronic Engineering, Firat University.